Nanoindentation on silicon surfaces

R. Astala, M. Kaukonen and R. M. Nieminen
Laboratory of Physics, Helsinki University of Technology, P.O. Box 1100, FIN-02015, Finland

T. Heine
Institut für Teoretische Physik, Technische Universität Dresden

We investigate the atomic-scale details of atomic force microscopy (AFM) by using a quasistatic molecular dynamics simulation together with a density-functional based tight-binding (DFTB) method. The changes in the AFM-tip shape, the size of the tip-sample contact area, as well as the microscopic hardness and Young's moduli of silicon {111}, {110}, {100} surfaces are studied. Furthermore, the effects of hydrogen termination of the surface and of sub-surface vacancies on the hardness and Young's modulus are discussed.

61.16, 62.20, 68.10

I. INTRODUCTION

Atomic force microscopy has become a standard tool in experimental surface physics, revealing atomic scale structures of surfaces. Manipulation by an AFM-tip has also been successful [1]. Experimental work has also been carried out to obtain information of macroscopic quantities, such as hardness, Young's modulus and the shear modulus of the surface. These quantities can be estimated based on the force curves obtained from the AFM-experiments [2,3].

Ab initio calculations have been made to clarify the changes in the electrical and atomic structure during nanoindentation, i.e. the pushing the AFM-tip into the surface and pulling it back to its original position on Cu{110}, Au{100} and Si{111} surfaces [4–6]. These studies show that an AFM (or a scanning tunneling microscope [STM]) tip can extract atoms from the surface and cause a plastic deformation of the substrate. It is found that the changes in the electron distribution precede the changes in the atomic configuration. Shluger et al. (Ref. [7]) have studied the non-contact-mode of AFM on ionic LiF, NaCl, and MgO surfaces using an embedded-cluster Hartree-Fock method. They find that the tip causes surface deformation or even neck formation between tip and surface. The energy barriers on the surface are shown to be reduced due to the tip in the vicinity of the surface. Furthermore electron tunneling from the tip to the surface is observed [7].

Classical simulations have focused on the AFM force curves (i.e. the force acting on the AFM-tip as function of the indentation depth) and explaining the atomic response of the surface during the AFM-measurement. Furthermore, these simulations give insight in surface friction properties and reveal the stick-slip type of tip motion during horizontal-scanning AFM, for example on the MoS_2{0001} surface [10]. The contact area between the tip and the surface has been approximated within continuum mechanics by Lantz et al. for various systems, with good results for metal-tip metal-substrate systems [8].

The influence of a metal tip (Ni) shape on the metal (Cu{110}) surface has been evaluated by Buldum et al. They find that the tip shape affects both the type of jump that the tip makes to the contact and the localization of surface deformation. They discover a connective neck formation between the sample and the tip in some cases [11].

AFM simulations for Si{111} (2×1) Pandey chain surfaces with the density–functional theory (DFT) level of theory [6] or recently on Si{111} 5X5 with the DFT extended with Van der Waals contributions for the tip–surface interactions [9] have been performed. It is therefore interesting to compare these results with our DFTB calculations when there is overlap in the investigated properties. In this paper we try to give an overall picture of the AFM-measurement on Si{111} 2×1 Pandey chain, Si{100} 2×1 and Si{110} surfaces.

The organization of the paper is as follows. In Section II we describe the density–functional based tight– binding method (DFTB) as well the simulation geometries. The nanoindentation simulations are described in Sec. III. The results are given in Sec. IV. Finally a discussion and conclusions follow in Secs. V and VI.

II. THEORETICAL METHOD AND THE MODEL SYSTEM

The density–functional based tight–binding method (DFTB) derives its name from its use of self–consistent density–functional calculations for pseudo–atoms in order to construct transferable tight–binding (TB) potentials for a non–self consistent solution of the Kohn–Sham equations for the many body case. It differs from conventional tight–binding techniques in that there is a systematic way of deriving these potentials, independent of the atom type involved. This is thus not a "parametrisation" as is usually meant when discussing TB approaches. An excellent review article written by Goringe et al. summarizes the general theoretical basis of the tight–binding method and the current progress in the theory [12]. For an in–depth description of the DFTB, the reader is recommended to consult Ref. [13]. The detailed description of the apllication of DFTB for silicon is given in Ref. [15].

In this work we examine three silicon surfaces. The Si {100} (2×1) surface consists of eight layers of silicon atoms with in total 160 atoms in the unit cell. The Si {111} (2×1) buckled Pandey chain surface has 176 atoms in five double layers, and the Si {110} surface includes 168 atoms in six Si layers. All silicon atoms are allowed to move freely, except the fixed bottom layer. The dangling bonds at the bottom of the surface are saturated with immobile hydrogen atoms. The surfaces during AFM–measurements are depicted in Fig. 1. The dimensions of the super-cells in x-y (surface plane), and the slab height in z (surface normal) directions are:

{100} 15.35Å × 15.35Å × 9.6 Å
{110} 15.35Å × 16.28Å × 9.8 Å
{111} 13.30Å × 15.35Å × 13.7 Å

Both a sharp and a flat diamond tip are used in this work. The sharp tip has in total 40 atoms: 28 carbon atoms and 12 pseudo-hydrogens to saturate dangling bonds. The height in the surface normal direction of the undisturbed sharp tip from the apex to the uppermost carbon layer is 4.4 Å. The flat tip consists of 55 atoms of which 43 are carbons and 12 pseudo-hydrogens. Its height from the lowest to the uppermost carbon layer is about 2.4 Å. These tips are made by cutting a piece of unreconstructed diamond {111} surface and conjugate gradient (CG) relaxing the piece in order to find a minimum energy configuration. The tips are shown in Fig. 2.

The effect of hydrogen on the surface in AFM experiment is investigated with a hydrogen terminated {100}:H 2×1 surface. The influence of a single subsurface vacancy on the film properties is studied on the {100} and {111} surfaces.

III. SIMULATION DETAILS

In all simulations a push-pull (loading–unloading) AFM cycle is performed. The tip is pushed to 0.7 Å - −3.2 Å indentation depth and then pulled upwards.

The indentation depth is measured as the distance between the uppermost fixed carbon layer of the tip and the topmost atomic layer on the surface, minus the height of the undisturbed tip, i.e. the indentation depth z = 0 corresponds a situation where the undisturbed tip just touches the undisturbed surface. This depth is well-defined even if the tip is deformed. The simulation with the flat tip are performed using the depths of only 0.7 Å - −0.5 Å, in order to gain information not distorted by the effects resulting from the finite sizes of the surfaces in the z-direction. The maximum depth for the sharp tip is selected so that the fixed atoms on the top of the tip remain above the surface.

The simulations are performed using constant–volume conditions in the lateral planew. The tip (flat or sharp) is positioned so that the initial minimum distance in z-direction between the surface and tip atoms is 2.5 - 3.1 Å. It is pushed into the surface with steps of 0.1 a.u. (0.0529 Å). After each step, the system is conjugate gradient (CG) relaxed (corresponding to zero temperature) with two exceptional groups of atoms. Firstly the atoms at the bottom layer of the surface are kept fixed in order to prevent an all-atom movement of the super-cell. Also the pseudo-H's bonded to the bottom layer are kept fixed. Secondly, the two topmost layers of C atoms and the pseudo-H's of the AFM-tip are kept fixed in the surface normal direction in order to apply force to the system. The force acting on the AFM-tip is calculated by summing the z-components of forces acting on the individual tip atoms

$$F_z = \sum_{tip} F_{z_i} \tag{1}$$

This force is well defined because the number of C and pseudo-H atoms on the tip remains constant in every simulation.

In order to make the tip more stable, the topmost two C layers and the pseudo-H's are fixed relative to each other in the x-y plane. This is accomplished by calculating the z-component of the torque and the forces in the x-y - plane on the fixed tip atoms and then redistributing them as uniform acceleration and rotation on the x-y-plane. The torque is calculated as

$$\vec{\tau}_{fix} = \sum_{fix} (\vec{r}_i - \vec{r}_{cm_{fix}}) \times \vec{F}_i \tag{2}$$

and the fixed atoms are rotated according to

$$\vec{F}_{rot_i} = \vec{\tau}_{fix} \times \frac{\vec{r}_i - \vec{r}_{cm_{fix}}}{\sum_{fix} (\vec{r}_j - \vec{r}_{cm_{fix}})^2} \tag{3}$$

.

The contact area between the tip and the surface is estimated by calculating the number of bonds between the tip and the surface. An estimated area of 5.51 Å^2 per bond on diamond {111} surface is used.

IV. RESULTS

A. Tip shape and the contact area

1. General features

Apart from the case of the hydrogen-terminated surface, a small attraction between the surface and the tip is noticed during the pre-loading phase, i.e. before the tip-surface contact had been established. The attraction vanishes with the hydrogen-terminated surface because of the surface dipole (the surface hydrogen atoms are positively charged). After the unloading phase, there is a strong attraction of few $\frac{eV}{\AA}$, because of the bonds which have formed between the tip and the sample.

In most simulations the tip is deformed during the simulation. With the sharp tip the deformation is most severe on {110} and {111} surfaces. The number of Si atoms sticking to the tip after the simulation are shown in the Table I. As a general trend one can observe that surface an with energy–lowering reconstruction ({111}) is more resistant against the abstraction of surface atoms.

The deformation process of the surface begins when the tip approaches the contact regime. The outermost tip and surface atoms start to form bonds and they are slightly attracted towards each other. As the tip further approaches the surface, this attraction turns to repulsion when the atoms are forced closer to each other, with typical inter-atomic distance between Si-C pair being of order 2 Å. The surface atoms making bonds to the tip are homogeneously forced downwards deeper into the surface and the sample is further deformed. With the sharp tip and perfect surface, the deformation of the surface is restricted to the few uppermost atom layers on the surface.

Interstitials are detected with flat tip on all the three surfaces. The geometries of interstitials in bulk silicon are presented in Ref [20]. The ⟨110⟩ dumbbell interstitial is also described in Refs [21] and [22]. When interstitials start to form in our simulations, the uppermost Si layers typically are in amorphous state, and the pressure from these layers induces the interstitial formation at lower atomic layers. Since the crystal environment above these interstitials is in an amorphous state, these interstitials have unusual geometries which are cannot be classified as bulk interstitials presented in Ref [20].

The surface remains locally deformed after the indentation process mainly because of the Si atoms transferred to the tip. The maximum total contact area ranges from 39 to 77 $\AA^2$ with the sharp tip on the perfect Si surfaces. It increases slightly with the flat tip, Tab. I. The {100} surface has smaller values for the contact area than the other surfaces because of the resistant 2×1 reconstruction. The contact area typically increases strongly during the loading phase from almost zero value near its maximum value in a short distance. This increase takes place at indentation depth of 0 - 2 Å. The contact area as a function of indentation depth for clean surfaces and a flat tip are shown in Fig. 6. The increase is nearly monotonous, as the small jumps in the curve are likely to result from the method used in the evaluation of contact area.

2. {111}, {100}, {110} and (100:H) surfaces

Both Pandey chains on the {111} surface in our simulation cell reconstruct to the regular diamond-structure under the pressure from the flat tip. This is understandable because the AFM acts as a source of bonds for the under-coordinated surface atoms. Similar reconstruction of Pandey chains occurs also on the {111} surface with the sharp tip. In this case only the atoms in the Pandey chain under the tip undergo the 'phase transition' to diamond-structure. During the Pandey chain destruction the energy release for the reconstruction of one 7-ring to a 6-ring is of order 1 eV. The simultaneous change in the bonding of the tip atoms with the surface atoms contributes significantly to this energy.

The interstitial formation on the {111} surface is not clear. With the flat tip, four atoms in the second topmost double layer are pushed downwards from their original position towards interstitial positions.These atoms move deeper into the substrate more than 0.6 Å. Two of them move more distinctively, one moves to a ⟨110⟩ dumbbell-like position, while another moves to a interstitial position beneath the {111} layer (Fig. 1). However, there is no clear jump to the interstitial position, so it seems that the interstitials do not fully form. The dumbbell-like interstitial has different bond ordering than the usual ⟨110⟩ dumbbell and the bond lengths have differences when compared to *ab initio* calculations [22]. With the sharp tip, the behavior of downward movement is limited to two atoms and the movement is not so strong. When compared to Ref [6], the behavior of the sharp tip in the {111} surface has a similar feature of the upward flow of some surface Si atoms along the tip sides.

On the {110} surface with the flat tip, the formation of three dumbbell-type interstitials starts to take place on the indentation depths of 0.6 Å. This happens in the third silicon layer from the above. Because the surface directly above interstitials is in an amorphous state and the three interstitials are next to each other in a {110} chain, they cannot clearly be identified as {110} dumbbell interstitials. No interstitials are formed with the sharp tip on the {110} surface.

On the {100} surface with the flat tip, one Si atom is forced near the hexagonal interstitial position between the fifth and sixth layer. There is no clear jump to the interstitial position, and this interstitial vanishes, as the deformation of the surface proceeds. Also some dumbbell-type interstitials starts to form, but this behavior is not clear due to amorphisation of the surface.

In the simulations with hydrogen-terminated {100} the tip first goes on the top of the dimer chain between hydrogen atoms. This behavior is due to hydrogen atoms screening the energy minima between the dimer rows. The tip pushes one of the H atoms into the surface and starts to move between the dimer chains. Eventually the

H atom moves to a interstitial position in a third Si layer.

The sharp tip finds an energy minimum between the surface atom chains in the simulations on clean {100} and {110} surfaces. On the {111} surface, the tip does not go between the Pandey chains. Instead, the Pandey chains are reconstructed in the previously discussed manner.

3. {100} and {111} surfaces with a subsurface vacancy

The influence of a subsurface vacancy on the hardness is studied on the {100} surface with a single vacancy in the sixth silicon layer from the top of the surface, and on the {111} surface with a vacancy in the fourth double layer. The point group of the relaxed vacancy is nearly D_{2d}, i.e. the nearest neighbors of the vacancy have two short distances with each other and four lengths nearly equal

(2.9 Å, 2.9 Å)
(3.27 Å, 3.27 Å, 3.36 Å, 3.36 Å)

In the {111} vacancy the distances were

(3.19 Å, 3.34 Å, 3.52 Å, 3.52 Å, 3.55 Å, 3.55 Å)

In this case of the {100} surface and the vacancy the sharp tip does not go to the intermediate position between the dimer chains in the {100} plane, but remains near the top of the dimer row. This has an effect of slightly increasing the contact area. The surface is less deformed than in the case of plain {100} surface.

On the {111} surface the vacancy initially placed on the fourth double layer localizes in two neighboring lattice positions under the pressure from the tip. This occurs for the indentation depth of 0.8 Å. The energy gain associated with the vacancy splitting is 1.2 eV. In the splitting the atom above the vacancy moves downwards in the ⟨111⟩ direction to halfway between its original position and the empty lattice site, forming bonds with the other neighbouring atoms of the empty tetrahedral position. The atom shifts downwards below the halfway position as the pressure from the tip increases. Finally when the unloading is started, the atom does not return to its original position. Two bonds with its initial neighbors break, and the atom stays closer to the original vacancy site in the fourth double layer. This behavior is explained by the greater deformation of the next upper double layer, which reduces the binding energy of the atoms there, so it is energetically preferable for the atom to form bonds with the atoms in the lower double layer.

The reconstruction of the {111} surface occurs also with the vacancy. The energy gain is about the same as in the perfect surface.

B. Hardness and Young's modulus

The hardness of the substrate is calculated as

$$H = \frac{F_{max}}{A_{projected}}. \tag{4}$$

F_{max} is the maximum value of repulsive force measured during the loading and $A_{projected}$ is the corresponding projected contact area. For the geometry of a sharp tip

$$A_{projected} = 0.558 * A \tag{5}$$

The coefficient between the projected and the total contact area A_{flat} is derived from simple geometrical considerations by projecting the total area of the undeformed tip facing the surface to a plane. With the flat tip, the projected area is considered equal to the total contact area.

The ratio $\frac{F}{A_{projected}}$ for the surfaces (with the flat tip) is presented in Fig. 7. The points in the curve are calculated by computing $\frac{F}{A_{projected}}$ and then averaging over five neighboring depth. This is done in order to smooth out peaks in the force. The depths with attractive values of force or zero contact area, which would give unacceptable values for the $\frac{F}{A_{projected}}$, are rejected in the averaging.

As discussed above, the subsurface vacancy affects the penetration position of the AFM-tip on the xy-plane. The energetically favored penetration position on {100} surface with a vacancy is such that the contact area increases compared to ideal {100} surface thus decreases the hardness measured at low indentation depths. (See Tab. II).

The reconstruction of the Pandey chain structure on the {111} surface, using the flat tip has an effect of decreasing the steepness of the loading curve by about 60 %, due to the fact that there is no more surface reconstruction to be destroyed. During the less steep region, the force against the tip comes from the bond shortening of the bulk structure. Finally, the interstitial formation and the finite size of the sample start to take effect, and the loading curve steepens again. In the vacancy case, the final reconstruction of the second Pandey chain happenes approximately at the same depth as the final reconstruction of the remaining 7-atom rings beneath the tip. During this process, there is a strong jump in the loading curve, and the resisting force decreases by 55 % (Fig. 4). Otherwise the steepness of the loading curve is not significantly affected as in the simulation without the vacancy. During the jump, the increase in the number of 6-atom rings on the surface layer is more than three times greater than in the corresponding reconstructions in the undefected surface. In the tip-surface interface region, there are rings containing Si and C atoms. The number of carbon atoms taking part in the 6-atom and 5-atom rings is generally greater in the vacancy case during the jump.

During the unloading phase, the bonds between the surface and the tip atoms cause an attractive force between the tip and the sample (z > 0 region).

Young's modulus is calculated using the theory of Herzian contact

$$E^*_{sub} = \frac{\sqrt{\pi} S}{2\beta\sqrt{A}}, \quad (6)$$

where S is the unloading stiffness, ie. slope of the unloading curve, measured at the very beginning of the unloading phase [2].

β is a coefficient depending on the tip geometry and E^*_{sub} is the reduced modulus corresponding to the elastic response of both the tip and the surface. [2]. The value of $\beta = 1.012$ is used for the sharp tip because of its pyramidical geometry. For the flat tip $\beta = 1$ is considered most suitable, since its geometry is near circular [16]. The macroscopic Young's modulus E_{sub} is then derived from

$$\frac{(1-\nu^2_{sub})}{E_{sub}} = \frac{1}{E^*_{sub}} - \frac{(1-\nu^2_{tip})}{E_{tip}.} \quad (7)$$

E_{tip}, ν_{tip} and ν_{sub} are the Young's modulus of the tip, the Poisson ratio of the tip and the surface, respectively. Their numerical values are assumed to be well-known from experimental results: $E_{tip} = E_{diamond} = 1050$ GPa, $\nu_{tip} = \nu_{diamond} = 0.10$,$\nu_{sub} = \nu_{silicon} = 0.28$ [18]. The derivation of the Young's modulus assumes that all deformations are reversible i.e. elastic. For more detailed discussion of Hertzian theory about normal contact, see Ref. [19]. The calculated values for the Young's modulus for different surfaces are shown in Tab. III. We will discuss these results in the following section.

The maximum value of torque (Eq. 2) on the fixed atoms of the tip is of order $7 * 10^{-18}$ Nm. The torque typically oscillates around the zero value with an irregular fashion.

The influence of the finite size effect on hardness is tested making a low-depth simulation with a bigger super-cell,

(19.184 Å× 21.705 Å× 9.8 Å)

{110} surface with the flat tip. The evolution of the ratio $\frac{F}{A}$ is depicted in Fig. 9. The first maxima in the ratio is of order 15 % smaller with the bigger super-cell. However, the unloading stiffness S is for both sizes of the simulation cell near 13 $eV/Å^2$ This gives an implication that the unloading stiffness is a proper quantity to characterize the surfaces.

V. DISCUSSION

In all simulations there is adhesion between the tip and the surface. The small attraction at the beginning of the loading phase can be interpreted as the tip jumping to contact mode. The strong attractive force between the tip and the surface at the end of the unloading phase (z ≈ 2 with flat tips and z ≈ 2 with the sharp tips) is a result of a bond formation between the tip and the surface atoms (Figs. 3,4).

The indentation processes in all simulations are non-elastic. This can be seen from the hysteresis-like behavior of loading and unloading curves or by visually inspecting the surfaces and the tips after the indentation (Figs. 3, 4). The processes are not elasto-plastic in the classical sense, since adhesion between the surfaces due to the bond formation, and transfer of surface atoms to the tip are present.

The sharp tip deforms easily because of the large number of dangling bonds on the tip and the surface making the tip and surface atoms react strongly with each other. The flat tip is more resistant against deformations, because the smaller number of dangling bonds. The deformation of tips is consistent with the experimental results of destruction of diamond tips on contact-mode probing on SI surfaces [17].

The depth dependence of the ratio $\frac{F}{A}$ in Fig. 7 has maximum around the depth of -0.6 - 0.2 Å. On the {100} surface with the flat tip the sudden decrease in energy is associated with an interstitial formation in the subsurface region. In this transformation overcoordinated atoms recover back their sp^3 bonding and one hexagonal-like interstial is formed.

The ratio $\frac{F}{A}$ has lower values for the {111} surface+flat tip. This may be because the force on the tip has almost always smaller value during the loading on the {111} when compared to {100} and {110} surfaces in same depths. This can partly stem from the Pandey chain reconstruction, which causes a downward movement among the topmost surface atoms and effectively lowers the sample surface level. On the other hand, there is no clear local maximum in the $\frac{F}{A}$ with the {111}. This indicates that there is no large energy barrier assosiated to the Pandey chain- diamond reconstruction. The formed diamond structure is more resistant against interstitial formation compared to the {100} and {110} surfaces so this surface has no sudden drops in the energy curve (Fig. 8 as in the {100} case.

The extracted values of Young's modulus for the surface are in average of 70-220 % too high when compared to the experimental value of 130 GPa. However, using the DFTB for the computation of the Young's modulus by compressing bulk silicon gives a value of 137 GPa. We believe that the difference compared to the experimental values and our results can be understood as follows.

In the real experiment the indentation depth is much greater than in our simulations. In the simulations one is still in the nearly elastic region, while we believe that in the experiments one has local amorphisation and massive interstitial formation. As can be seen in Fig. 4 the the slope of the force curve still steepens in the deeper intendation depth, indicating nearly plastic behaviour. So in our simulation we are not deep enough to have a depth independent response from the surface. Furthermore, the reconstruction effects on the surface may also steepen the unloading curve and thus yield higher estimate for the Young's modulus.

The subsurface vacancy decreases Young's modulus as expected III. However, the simulated values for Young's modulus with the vacancy and the sharp tip are very sensitive to the initial x-y position of the tip. The vacancy affects the shape of the tip-surface energy landscape and thus the penetration position of the tip on the xy-plane. With reconstructions on the surface this leads to different contact areas and thus to different values for Young's modulus. When using the flat tip, the initial xy-position dependence is not strong. The simulation with the vacancy, using the sharp tip, gives about 18 % smaller value for the Young's modulus for the {100} surface, and 54 % smaller value for the hardness, compared to the surfaces without the vacancy. Interestingly the sudden drop in the force curve (Fig. 4) is associated with ring formation processes on the surface reconstruction and not near the vacancy itself (as discussed in Sec. IV A.3).

For the hydrogenated surface {100}:H 2×1 case, because of the small tip size, only a small fraction of the tip C atoms are able to make bonds with the Si atoms on the surface. We obtain, however, a decrease in the hardness and and Young's modulus. The minimum energy pathway between the dimer rows is blocked due to hydrogen on the surface, so the values with the flat tip would probably decrease less.

The zero-temperature simulation temperature may also affect the measured force. A higher temperature makes it less likely for the system to get trapped into some local energy minimum, so the force on the tip may decrease. However, the higher simulation temperature would increase the pressure of the system, which would in turn increase the forces acting on the tip.

VI. CONCLUSIONS

We have performed a density-functional based tight-binding quasi-static simulation of AFM processes in order to study the shape of the contact area, hardness and Young's modulus.

The contact area is found to depend on the indentation depth in a way that could imply jumping from non-contact to contact mode. This is implicated by a sudden increase in contact area under a short distance, and by a presence of a small attractive force during the pre-loading phase.

We have shown that a simulated AFM measurement can be used to identify the atomic rearrangements during the indentation. AFM can detect impurities on the surfaces and defects beneath the surface. We find that subsurface vacancies or hydrogen coverage of the surface decrease the hardness and Young's modulus. The numerical values for hardness and Young's modulus depend strongly on the tip shape and the indentation depth. Experimentally, instead of measuring Young's modulus with which requires a priori knowledge of the Poisson ratio of the surface and tip, a simple ratio of $\frac{\Delta F}{\Delta z}$ at the beginning of the unloading phase would better reflect the elastic response of the surface. Our results do not support the use of Eq. 6 in determining Young's modulus of the surface.

Finally, we make a speculative proposition for the tip-surface interactions during an AFM-measurement. It is speculative because in the simulations the tip penetrated maximally only few Å into the surface. However, our suggestion is as follows: i) The tip experiences an attractive force to the surface basically due to the unsatisfied bonds on the surface and in the tip. ii) The surface reconstruction is destroyed because the AFM tip atoms act as a source of new bonds, and also the pressure from the tip destroys the surface reconstruction. iii) The bonds below the top surface layers are globally shortened. iv) Interstitials and vacancies are formed in the subsurface layers. v) Amorphisation takes place in the vicinity of the tip. One could therefore infer the bulk properties by examining the force curves on the region 3).

[1] J. A. Stroscio and D. M. Eigler, Science **254**, 1320 (1991); M. F. Crommie, C. P. Lutz, and D. M. Eigler, Science **262**, 218 (1993).
[2] D. M. Schaefer, A. Patil, R. P. Andres, and R. Reifenberger Phys. Rev. B **51**, 5322 (1995).
[3] M. Radmacher, R. W. Tillmann, M. Fritz, and H. E. Gaub, Science **257**, 1900 (1992).
[4] S. Ciraci, E. Tekman, A. Baratoff ,and I. Batra, Phys. Rev. B **46**, 10411 (1992).
[5] M. Sorensen, K. Jacobsen ,and H. Jonsson, Phys. Rev. Lett. **77**, 5067 (1996).
[6] R. Pĕrez, M. Payne ,and A. Simpson, Phys. Rev. Lett. **75**, 4748 (1995).
[7] A. L. Shluger, L. N. Kantorovich, A. I. Livshits and M. J. Gillan Phys. Rev. B **56**, 15332 (1997).
[8] M. A. Lantz, S. J. O'Shea and M. E. Welland, Phys. Rev. B **56**, 15345 (1997).
[9] R. Pĕrez, I. Štich, M. Payne ,and K. Terakura, Phys. Rev. B **58**, 10835 (1998).

[10] S. Fujisawa, E. Kishi, Y. Sugawara, and S. Morita, Phys. Rev. B **51**, 7849 (1995).

[11] A. Buldum, S. Ciraci and I. P. Batra, Phys. Rev. B **57**, 2468 (1998).

[12] C. M. Goringe, D. R. Bowler and E. Hernándes, Rep. Prog. Phys. **60**, 1447 (1997).

[13] D. Porezag, Th. Frauenheim, Th. Köhler, G. Seifert and R. Kaschner, Phys. Rev. B **51**, 12947 (1995).

[14] Th. Frauenheim, F. Weich, and G. Seifert, Phys. Rev. B **52**, 11492 (1995).

[15] M. Kaukonen, P. K. Sitch, G. Jungnickel, D. Porezag, S. Pöykko, R. M. Nieminen, and Th. Frauenheim, Phys. Rev. B, **57**, 9965 (1998).

[16] G.M. Pharr, W.C. Oliver, F.R. Brotzen, J. Mater. Res. **7**, 613 (1992).

[17] T. Uchihashi, Y.Sugawara, T. Tsukamoto, M. Ohta, S. Morita and M. Suzuki, Phys. Rev. B **56**, 9834 (1997).

[18] C. T. Lynch, CRC Handbook of Materials Science, Vol III, 4th ed. (CRC Press 1986)

[19] K.L Johnson, Contact Mechanics, (Cambridge University Press 1985)

[20] J.-L. Mozos, R. M. Nieminen, Self-interstitials in silicon: structure and migration mechanisms, in Properties of crystalline silicon, ed. Robert Hull, EMIS, London 1998.

[21] Meijie Tang, L. Colombo, Jing Zhu and T. Diaz de la Rubia, Phys. Rev. B **55**, 14279 (1997).

[22] S. J. Clark and G. J. Ackland Phys. Rev. B **56**, 47 (1997).

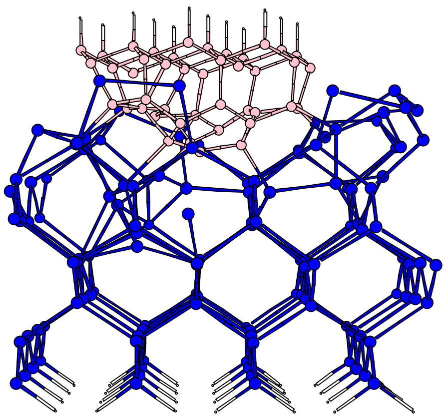

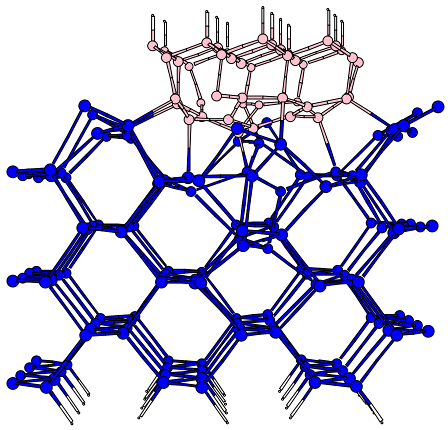

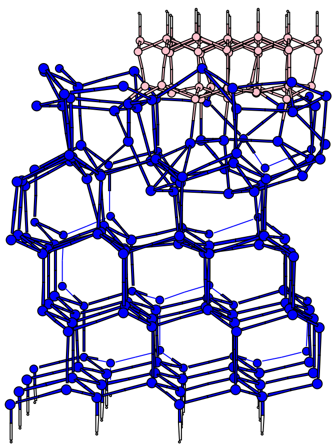

FIG. 1. The flat tip indenting different surfaces. Si-surfaces from top: {100}, {110}, {111}. The formation of an amorphous layer near the tip and a region with interstitials below the amorphous layer is observed.

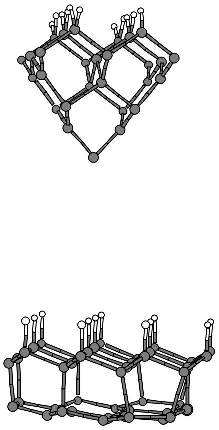

FIG. 2. The sharp and flat tips. The sharp tip has totally 40 atoms, 28 C and 12 pseudo H to saturate dangling bonds. The flat tip consists of 55 atoms (43 C, 12 pseudo-H). The tips are generated by cutting a piece of diamond in the {111} direction, saturating the upper surface with pseudo-H and thereafter conjugate gradient relaxing.

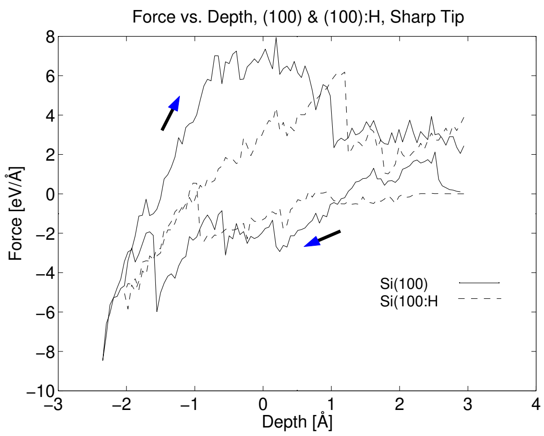

FIG. 3. The depth (Å) dependence of force (eV/Å) on the clean (solid line) and hydrogenated {100} (dashed line) surfaces when indenting with the sharp tip. The lower portion of the curve displays the loading and the upper portion the unloading phase. The arrows also indicate the direction of the simulation.

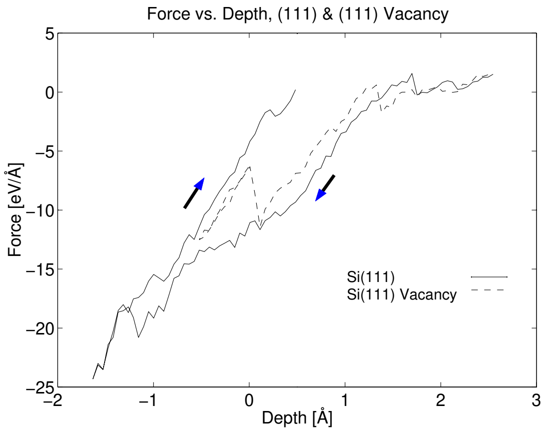

FIG. 4. The depth (Å) dependence of force (eV/Å) on the clean {111} (solid line) and {111} with a vacancy (dashed) surface when indenting with the flat tip. The lower portions of the curves display the loading and the upper portion the unloading phase. Around the zero depth the figure displays the less steep region on the plain surface curve and the peak in the force on the vacancy curve.

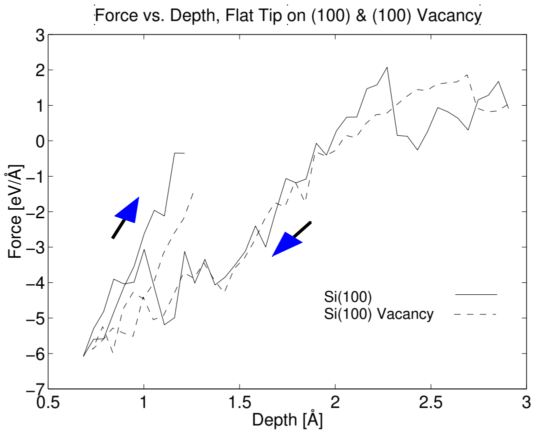

FIG. 5. The depth (Å) dependence of force (eV/Å) on the {100} surface with and without the vacancy when indenting with the flat tip. The solid curve displays the clean and the dashed curve the vacancy case.

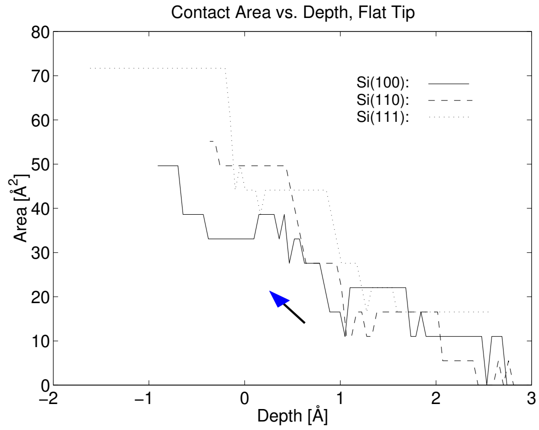

FIG. 6. Development of contact area (Å^2) vs. indentation depth (Å) for the flat tip indenting Si {100} (solid line), {110} (dashed line) and {111} (dotted line).

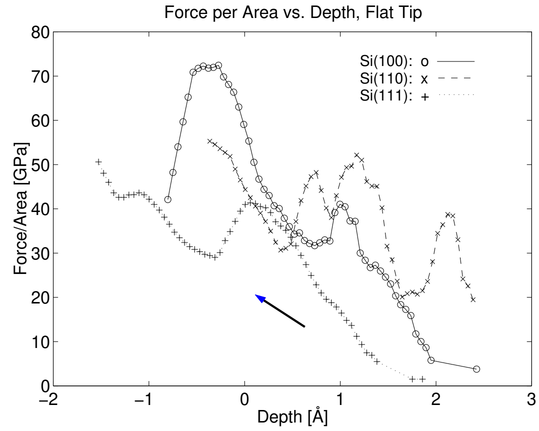

FIG. 7. Development of force / area (GPa) vs. indentation depth (Å) for the flat tip indenting Si {100} (solid line), {110} (dashed line) and {111} (dotted line).

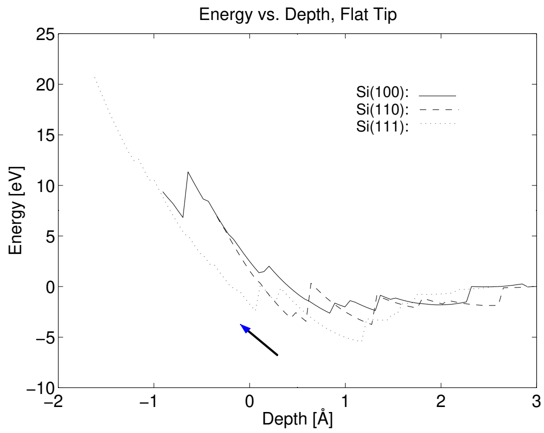

FIG. 8. Development of energy (eV) vs. indentation depth(Å) for the flat tip indenting Si {100} (solid line),{110} (dashed line) and {111} (dotted).

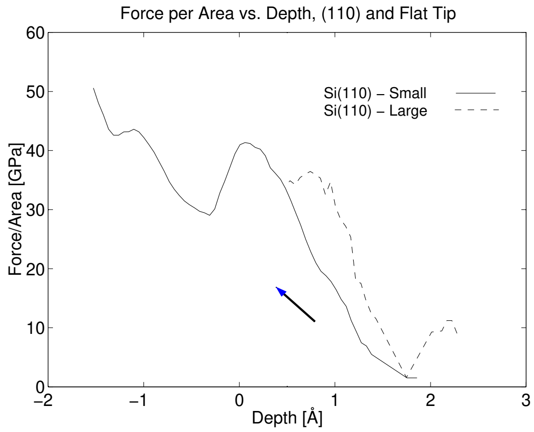

FIG. 9. Development of force / area (GPa) vs. indentation depth(Å) for the flat tip indenting small (solid line) and large (dashed line) {100} surface.

TABLE I. Transferred atoms and maximum total contact area for the deepest indentations (Å^2). The contact areas in the table are the maximum values over all indentation depths.

Tip, Surface	Atoms Transferred	Contact Area
Sharp tip, {100}	8	50
Sharp tip, {110}	8	77
Sharp tip, {111}	4	66
Sharp tip, {100}, vacancy	6	61
Sharp tip, {100}:H	0	39
Flat tip, {100}	-	50
Flat tip, {110}	17	88
Flat tip, {111}	2	72
Flat tip, {100}, vacancy	-	28
Flat tip, {111}, vacancy	-	72

TABLE II. Hardness in different simulations

Tip, Surface	Depth	Hardness
Sharp tip, {100}	-1.8 Å	52 GPa
Sharp tip, {100}, vacancy	-1.8 Å	28 GPa
Sharp tip, {110}	-1.8 Å	47 GPa
Sharp tip, {111}	-1.8 Å	89 GPa
Sharp tip, {100}:H	-1.8 Å	43 GPa
Flat tip, {100}	-0.9 Å	57 GPa
Flat tip, {100}, vacancy	0.7 Å	43 GPa
Flat tip, {110}	0.4 Å	36 GPa
Flat tip, {111}	-0.4 Å	30 GPa
Flat tip, {111}, vacancy	-0.4 Å	28 GPa

TABLE III. Young's modulus: $E_{exp} = 130$ GPa There are two values for some of the flat tip indentations from two maximum depths.

Tip, Surface	depth	Young's modulus
Sharp tip, {100}	-2.3	397 GPa
Sharp tip, {100}, vacancy	-1.8	325 GPa
Sharp tip, {110}	-2.2	296 GPa
Sharp tip, {111}	-3.2	334 GPa
Sharp tip, {100}:H	-2.0	220 GPa
Flat tip, {100}	0.7 / -0.9	382/193 GPa
Flat tip, {100}, vacancy	0.7	252 GPa
Flat tip, {110}	0.3	323 GPa
Flat tip, {111}	-0.4 / -1.6	260 / 414 GPa
Flat tip, {111}, vacancy	-0.5	219 GPa